

# Water-like fluid in the presence of Lennard–Jones obstacles: predictions of an associative replica Ornstein–Zernike theory<sup>☆</sup>

T. Urbic<sup>a</sup>, V. Vlachy<sup>a,\*</sup>, O. Pizio<sup>b</sup>, K.A. Dill<sup>c</sup>

<sup>a</sup>Faculty of Chemistry and Chemical Technology, University of Ljubljana, Askerceva 5, 1000 Ljubljana, Slovenia

<sup>b</sup>Instituto de Química de la UNAM, Circuito Exterior, Coyoacán, México DF 04510, Mexico

<sup>c</sup>Department of Pharmaceutical Chemistry, University of California at San Francisco, San Francisco, CA 94143–1204, USA

## Abstract

What are the properties of water in the presence of a ‘sea’ of inert obstacles? This question arises because biological cells are highly crowded media, and it is of interest to know the properties of water inside them. It also arises for understanding water in confined molecular environments and for mixtures of water with non-polar solutes. We study two-dimensional Mercedes–Benz (MB) water that is freely mobile in a disordered, but fixed, matrix of Lennard–Jones disks. We use the associative replica Ornstein–Zernike equations supplemented by the corresponding hypernetted chain approximation, and we tested the theory using Monte Carlo simulations. We find that the structure of model water is perturbed by the presence of the obstacles. When the density of obstacles is small, the obstacles induce an increased ordering and ‘hydrogen bonding’ of the MB model molecules and increased compressibility, relative to pure fluid, in agreement with previous theoretical and experimental studies. However, interestingly, high obstacle densities reduce MB water structuring, ‘hydrogen bonding’, and compressibility, because the obstacles interfere so extensively with all the possible ways that the fluid can form good ‘hydrogen bonding’ networks.

© 2003 Elsevier B.V. All rights reserved.

PACS: 61.20.-p; 02.30.Rz

**Keywords:** Model of water; Partly quenched system; Lennard–Jones obstacles; Replica Ornstein–Zernike integral equation; Hypernetted chain approximation

## 1. Introduction

Confined water can be found in many natural environments [1,2], including those in biology. Biological cells are highly crowded media at the molecular level. It is of interest to know the properties of water in such environments [3,4]. In pure liquid water, i.e. at room temperature or below, water has extensive hydrogen bond network structure. However, if water is confined between planes, or in microscopic spherical or cylindrical pores, its structure and thermodynamic properties can be perturbed. Such a confinement has been extensively studied by experiments and theory. A partial list of recent work is in Refs. [5–17]. For example, exper-

imental studies show that confined water molecules have less mobility than unconfined water (see, for example, Ref. [9]). Here, we study water that is confined by being embedded within a matrix of fixed obstacles. The matrix is created in the model by a rapid quench of a Lennard–Jones fluid. Hence, this differs from the above studies in that our confinement is not due to a regular simple geometry. Our model has heterogeneity at the molecular scale. It is a disordered porous medium. The combined system of water plus obstacles can be regarded as a partly-quenched (PQ) system; i.e. some degrees of freedom are quenched (those of the Lennard–Jones matrix, in this case) and some are allowed to fully equilibrate (the model water). This system is not identical to a liquid mixture of particles, since the LJ system is frozen and is not free to equilibrate with the water. Theoretical methods for a description of partly-quenched mixtures are still in development and the progress has been reviewed recently [18–20]. The liq-

<sup>☆</sup>This paper is dedicated to Prof. Myroslav F. Holovko on the occasion of his 60th birthday honoring his contribution to the theory of strongly interacting systems.

\*Corresponding author.

E-mail address: vojko.vlachy@uni-lj.si (V. Vlachy).

uid-state statistical mechanics work of Madden and Glandt [21,22], Given and Stell [23–25], and others (see, for example, Refs. [26–29]) has paved the road for studying the properties of PQ systems. Their work has led to a formulation of the replica Ornstein–Zernike (ROZ) equations and its associated closure relations.

Our model system consists of two subsystems. The first one is a quenched fluid of Lennard–Jones (LJ) disks, called the matrix. We assume that the distribution of matrix particles is given by the solution of the integral equation (or, alternatively, from computer simulation) of the Lennard–Jones disk system at temperature  $T_0$ . The second subsystem is our model water, which thermally equilibrates in the presence of matrix particles at temperature  $T_1$ . The matrix particles do not respond to the presence of the annealed fluid (water). To calculate the thermodynamic properties of the system, we use a double ensemble average: first, we average over the annealed degrees of freedom (the model water, in the presence of fixed obstacles), then over all the possible values of the quenched variables (the obstacle distributions). Physically, this means that mobile fluid particles will visit all the representative domains of the matrix material. This necessarily makes computer simulations of partly-quenched systems very time consuming.

The model of water that we use here is the Mercedes–Benz model, originally proposed by Ben–Naim [30,31]. This model has recently been studied using NPT Monte Carlo simulations [32–36] and by thermodynamic-perturbation and integral equation techniques [37–39]. MB ‘molecules’ are two-dimensional Lennard–Jones disks with three radial arms to mimic the hydrogen bonds (HB), being arranged as in the Mercedes–Benz logo. Simulations have shown that the MB model qualitatively predicts many properties of real water, among them the density anomaly, the minimum in the isothermal compressibility as a function of temperature, and the thermodynamics of non-polar solvation [34]. An advantage of this simple model, compared to more realistic water models, consists in the fact that well converged computer simulations of thermodynamic properties can be obtained in a reasonable amount of time [33–36].

Here, we study MB water in the presence of LJ obstacles using the associative replica Ornstein–Zernike (ARoz) equations, in the corresponding hypernetted chain approximation [40]. By finding numerical solutions of the set of integral equations, we obtain the correlation functions and the fraction of MB water molecules that are hydrogen bonded. From the correlation functions, we calculate the excess internal energy and compressibility. Therefore, the main goal of this contribution is to determine the differences in structural and thermodynamic properties of a model fluid, brought about by the presence of the Lennard–Jones obstacles. The associative replica Ornstein–Zernike calculations were tested using Monte Carlo simulations of few

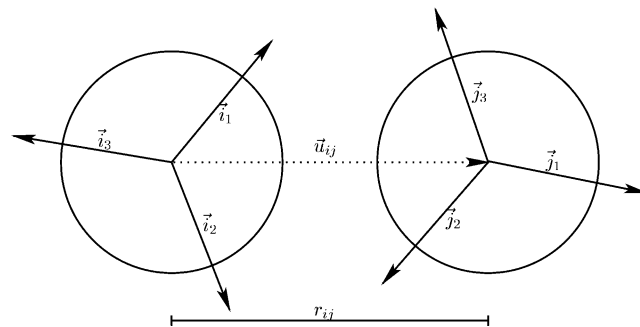


Fig. 1. Two MB model water molecules separated by a distance  $r$ .

representative examples in the canonical ensemble. The advantage of the AROZ, compared to Monte Carlo, is that it is orders of magnitude faster to compute.

There are two relevant preceding studies. Firstly, Kovalenko and Pizio [41] studied a model for a network-forming associating fluid in which each particle has four bonding sites. They calculated the adsorption isotherms for this fluid in the hard-sphere matrix using the associative replica Ornstein–Zernike theory. The liquid–vapor coexistence line was evaluated and compared with the result for the bulk fluid. Secondly, Kovalenko and Hirata [42] developed a replica interaction-site model theory to study a water-like fluid in a disordered microporous material. A key conclusion of their study is that, in qualitative agreement with experiment [8], confined model water exhibits enhanced hydrogen bonding.

## 2. The model

Here, we use the MB model of water [30–39]. Each Mercedes–Benz water molecule is a Lennard–Jones disk with three arms, which are separated by an angle of  $120^\circ$  (see Fig. 1). The model water mimics the open tetrahedral lattice form of ice found in real water with a two-dimensional honeycomb lattice [33]. The interaction potential between two MB molecules is a sum of a Lennard–Jones part and the term mimicking the hydrogen bond (HB) contribution

$$U(\vec{X}_i, \vec{X}_j) = U_{\text{LJ}}(r_{ij}) + U_{\text{HB}}(\vec{X}_i, \vec{X}_j) \quad (1)$$

where  $r_{ij}$  is the distance between the centers of molecules  $i$  and  $j$ , and  $\vec{X}_i$  denotes the vector representing the coordinates and the orientation of the  $i^{\text{th}}$  particle. The Lennard–Jones part of the potential is defined as:

$$U_{\text{LJ}}(r_{ij}) = 4\varepsilon_{\text{LJ}} \left[ \left( \frac{\sigma_{\text{LJ}}}{r_{ij}} \right)^{12} - \left( \frac{\sigma_{\text{LJ}}}{r_{ij}} \right)^6 \right] \quad (2)$$

where  $\varepsilon_{\text{LJ}}$  is the depth of the well and  $\sigma_{\text{LJ}}$  is the contact

parameter. The HB part of the interaction potential is:

$$U_{\text{HB}}(\vec{X}_i, \vec{X}_j) = \sum_{k,l=1}^3 U_{\text{HB}}^{kl}(r_{ij}, \theta_i, \theta_j), \quad (3)$$

where  $U_{\text{HB}}^{kl}$  describes the interaction between two arms of different molecules

$$U_{\text{HB}}^{kl}(r_{ij}, \theta_i, \theta_j) = \varepsilon_{\text{HB}} G(r_{ij} - r_{\text{HB}}) G(\vec{i}_k \vec{u}_{ij} - 1) G(\vec{j}_l \vec{u}_{ij} + 1). \quad (4)$$

By writing down the scalar products explicitly, we obtain the following form of the HB potential

$$U_{\text{HB}}^{kl}(r_{ij}, \theta_i, \theta_j) = \varepsilon_{\text{HB}} G(r_{ij} - r_{\text{HB}}) G\left(\cos\left(\theta_i + \frac{2\pi}{3}(k-1)\right) - 1\right) \times G\left(\cos\left(\theta_j + \frac{2\pi}{3}(l-1)\right) + 1\right), \quad (5)$$

where  $k$  and  $l$  stand for the different arms ( $A=1$ ,  $B=2$ , and  $C=3$ ) and  $G(x)$  is an un-normalized Gaussian function

$$G(x) = \exp\left(-\frac{x^2}{2\sigma^2}\right). \quad (6)$$

$\varepsilon_{\text{HB}}$  is an energy parameter and  $r_{\text{HB}}$  is a characteristic ‘hydrogen bond’ length.  $\vec{u}_{ij}$  is the unit vector along  $\vec{r}_{ij}$  and  $\vec{i}_k$  is the unit vector representing the  $k$ th arm of the  $i$ th particle, where  $\theta_i$  is the orientation of  $i$ th particle as shown in Fig. 1. In short, the strongest ‘hydrogen bonding’ occurs when an arm of one particle is co-linear with an arm of another particle, with the two arms pointing towards each other. The width of the Gaussian is small enough ( $\sigma=0.085 \cdot r_{\text{HB}}$ ) such that a direct bond is more favorable than a bifurcated one. Since the three HB arms of one particular MB molecule are labelled  $A$ ,  $B$  and  $C$ , that molecule can be in any one of eight different states: i.e. it can have zero ‘hydrogen’ bonds with other molecules, or a single bond,  $A-$ ,  $B-$ ,  $C-$ , two bonds,  $AB-$ ,  $AC-$ ,  $BC-$ , or it can have all three bonds,  $ABC-$ . Note that since the three arms are equivalent, the number of distinguishable states is four: each fluid molecule forms 0, 1, 2 or 3 bonds with neighboring fluid molecules.

Molecules of the matrix are modelled as Lennard–Jones disks without HB arms. The matrix–matrix interaction is described by Eq. (2). The standard Lorentz–

Berthelot rules [43] were assumed in calculating the matrix–fluid and matrix–matrix interactions.

### 3. Theory

#### 3.1. Associative replica OZ equation

The notation used to describe the partly-quenched system is as used before [40]: the superscripts 0 and 1 correspond to the matrix and the annealed fluid species, respectively. The associative ROZ equations can be written in the following form

$$h^{00}(r_{12}) = c^{00}(r_{12}) + \rho^0 \int c^{00}(r_{13}) h^{00}(r_{32}) d\vec{r}_3 \quad (7)$$

for the matrix–matrix correlations, and

$$h_i^{10}(r_{12}) = c_i^{10}(r_{12}) + \rho^0 \int c_i^{10}(r_{13}) h^{00}(r_{32}) d\vec{r}_3 + \sum_{kl} \rho_{kl}^1 \int c_{ik}^{11,c}(r_{13}) h_l^{10}(r_{32}) d\vec{r}_3. \quad (8)$$

for the fluid–matrix correlations. In these equations,  $h$  and  $c$  denote the partial correlation functions for various pairs of particles and  $\rho^0$  is equal to the density of LJ particles ( $\rho^0 = \rho_0$ ). As in our previous studies [37–39], we use the partial correlation functions that remain finite upon the decrease of the temperature; the details are explained elsewhere [37,44]. The fluid–fluid correlations are described by the equations

$$h_{ij}^{11}(r_{12}) = c_{ij}^{11}(r_{12}) + \rho^0 \int c_i^{10}(r_{13}) h_j^{01}(r_{32}) d\vec{r}_3 + \sum_{kl} \rho_{kl}^1 \int [c_{ik}^{11,c}(r_{13}) h_l^{11}(r_{32}) + c_{ik}^{11,b}(r_{13}) h_l^{11,c}(r_{32})] d\vec{r}_3 \quad (9)$$

and

$$h_{ij}^{11,c}(r_{12}) = c_{ij}^{11,c}(r_{12}) + \sum_{kl} \rho_{kl}^1 \int c_{ik}^{11,c}(r_{13}) h_l^{11,c}(r_{32}) d\vec{r}_3. \quad (10)$$

Next, the partial correlation functions are broken into blocked ( $b$ ) and connected ( $c$ ) parts

$$h_{ij}^{11}(r) = h_{ij}^{11,b}(r) + h_{ij}^{11,c}(r), \quad (11)$$

$$c_{ij}^{11}(r) = c_{ij}^{11,b}(r) + c_{ij}^{11,c}(r). \quad (12)$$

The blocking term corresponds to the correlations between the two particles that belong to different replicas. These particles do not interact directly with each other but they are correlated due to the presence of matrix particles. The lower index 0 stands for non-bonded molecule of water and 1 stands for the bonded one. We restrict ourselves to the so-called ‘ideal network’ approximation, which neglects all the partial correlation functions in which at least one of the indices is  $i, j \geq 2$  [45]. Physically, this means that we neglect the part of correlation responsible for the formation of the ring-like structures (cf. Fig. 1 of Vakarín et al. [45]). Taking into account the equivalence of the bonding arms, the matrix of fluid densities in Eqs. (8)–(10) has the following form [37]

$$\rho^1 = \begin{pmatrix} \rho_1 & 3\rho_1 \\ 3\rho_1 & 6\rho_1 \end{pmatrix}, \quad (13)$$

where  $\rho_1$  is the fluid density. The matrix of the correlation functions is  $z_{ij}^{11}$  where  $z$  stands for  $c$  or  $h$  is

$$\hat{z} = \begin{pmatrix} z_{00}^{11}(k) & z_{01}^{11}(k) \\ z_{10}^{11}(k) & z_{11}^{11}(k) \end{pmatrix}. \quad (14)$$

The symmetry relations for the correlation functions imply that

$$z_{10}^{11} = z_{01}^{11}; \quad z_j^{01} = z_j^{10}. \quad (15)$$

In order to solve the system of replica Ornstein–Zernike equations, additional relations between the  $h$  and  $c$  correlation functions are needed. In the present study we choose to examine the associative hypernetted-chain (AHNC) closure [46]. In this case, the regular HNC approximation

$$c^{00}(r) = \exp(-\beta_0 U_{\text{LJ}}^{00} + t^{00}(r)) - 1 - t^{00}(r) \quad (16)$$

is used for the matrix–matrix correlation, where  $t = h - c$ . As usual,  $\beta_0 = \frac{1}{k_B T_0}$ ; note again that  $T_0$  is the temperature of matrix preparation, and  $T_1$  is the temperature of observation. For the fluid–matrix correlation functions we use  $(\beta_1 = \frac{1}{k_B T_1})$

$$\begin{aligned} c_0^{10}(r) &= \exp(-\beta_1 U_{\text{LJ}}^{10} + t_0^{10}(r)) - 1 - t_0^{10}(r), \\ c_1^{10}(r) &= \exp(-\beta_1 U_{\text{LJ}}^{10} + t_0^{10}(r)) t_1^{10}(r) - t_1^{10}(r) \end{aligned} \quad (17)$$

and finally for the fluid–fluid correlations:

$$\begin{aligned} c_{00}^{11}(r) &= \exp(-\beta_1 U_{\text{LJ}}^{11} + t_{00}^{11}(r)) - 1 - t_{00}^{11}(r), \\ c_{10}^{11}(r) &= \exp(-\beta_1 U_{\text{LJ}}^{11} + t_{00}^{11}(r)) t_{10}^{11}(r) - t_{10}^{11}(r), \\ c_{11}^{11}(r) &= \exp(-\beta_1 U_{\text{LJ}}^{11} + t_{00}^{11}(r)) [t_{10}^{11}(r) \\ &\quad \times t_{01}^{11}(r) + t_{11}^{11}(r) + x^2 \bar{f}_{\text{HB}}(r)] - t_{11}^{11}(r). \end{aligned} \quad (18)$$

In Eq. (18),  $\bar{f}_{\text{HB}}(r)$  is the orientation-averaged Mayer function for the HB part of potential (Eq. (3)), and  $x$  is the fraction of the non-bonded molecules, obtained from the mass-action law [47,48] in the form

$$x = \frac{1}{1 + 3\rho_1 x \Delta} \quad (19)$$

where  $\rho_1$  is number density of MB molecules and  $\Delta$  is defined as

$$\Delta = 2\pi \int g_{00}^{11}(r) \bar{f}_{\text{HB}}(r) r dr. \quad (20)$$

The associative HNC closure for the blocked part of the direct correlation functions is

$$\begin{aligned} c_{00}^{11,b}(r) &= \exp(t_{00}^{11,b}(r)) - 1 - t_{00}^{11,b}(r), \\ c_{10}^{11,b}(r) &= \exp(t_{00}^{11,b}(r)) t_{10}^{11,b}(r) - t_{10}^{11,b}(r), \\ c_{11}^{11,b}(r) &= \exp(t_{00}^{11,b}(r)) \\ &\quad \times [t_{10}^{11,b}(r) t_{01}^{11,b}(r) + t_{11}^{11,b}(r)] - t_{11}^{11,b}(r). \end{aligned} \quad (21)$$

The solution of the associative ROZ equations yields partial fluid–matrix and matrix–matrix pair correlation functions. Their linear combinations correspond to the total pair correlation functions

$$g^{11}(r) = g_{00}^{11}(r) + 3g_{01}^{11}(r) + 3g_{10}^{11}(r) + 9g_{11}^{11}(r) \quad (22)$$

$$g^{10}(r) = g_0^{10}(r) + 3g_1^{10}(r). \quad (23)$$

We have made one additional approximation here. We use the orientationally averaged version of the Ornstein–Zernike equation for the MB model, whereby we average over all the intramolecular angles between the arms, rather than keep them at the fixed  $120^\circ$ . We have previously tested this approximation against the more exact orientation-dependent associative OZ approach [39], and Monte Carlo simulations of this model [33–36]. The numerical solution of the ROZ equations (Eqs. (7)–(10)) according to the closure conditions given above was obtained by a direct iteration. The forward

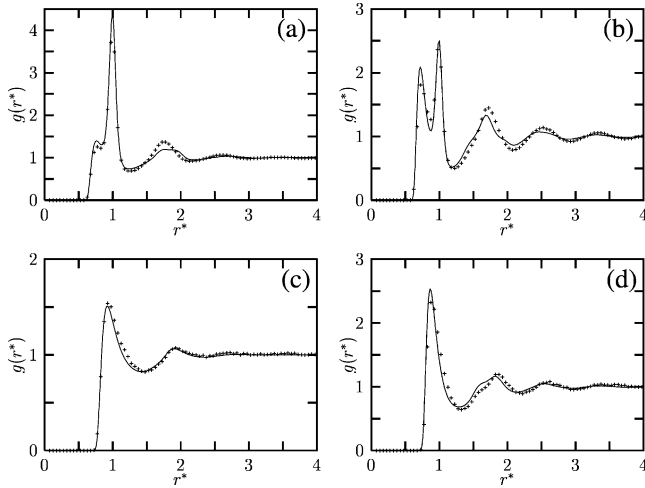


Fig. 2. The fluid–fluid distribution functions for  $T_0^* = T_1^* = 0.24$ ,  $\rho_0^* = 0.2$ , and  $\sigma_{\text{LJ}}^{00} = 1.0r_{\text{HB}}$ ; (a)  $\rho_1^* = 0.4$ , (b)  $\rho_1^* = 1.0$ . The fluid–matrix distribution (c)  $\rho_1^* = 0.4$ , and (d)  $\rho_1^* = 1.0$ . The Monte Carlo data are given by symbols.

and inverse Bessel–Fourier transforms, needed to couple the correlation functions in real and Fourier spaces, have been performed by the method of Talman [49].

### 3.2. Monte Carlo simulations

The method for computer simulation of partly-quenched systems has been discussed elsewhere [50–54]. The configurational properties must be obtained by first averaging over the annealed degrees of freedom and then also over all possible matrix configurations. Fortunately, a small number of equilibrium matrix realizations seems to be sufficient to obtain converged results [52–54].

The simulation procedure consists of two steps. In the first step we used the canonical Monte Carlo method [55] to simulate the Lennard–Jones matrix fluid. The number of matrix particles used in the simulations was 80. The matrix subsystem was equilibrated over  $10^6$  attempted configurations. In the next step, the mobile fluid molecules were introduced into the matrix and subjected to the usual canonical sampling procedure [55]. The number of annealed fluid molecules, distributed within the representative equilibrium realization of the matrix, varied from 160 (at low fluid concentration) to 400 (high fluid concentration). These MB molecules were first equilibrated over the  $10^6$  states. After this equilibration, a production run of  $10^7$  attempted configurations was performed to obtain the statistics as shown in figures. A new simulation cycle was started by changing the equilibrium distribution of the quenched LJ fluid (no annealed fluid particles were present during this part of the procedure) by running an additional  $10^6$  configurations. The final configuration was chosen

as the next representative distribution of matrix particles. At this stage, the MB model particles were introduced in the matrix again and, with the matrix particles fixed in their positions, the canonical averaging process was repeated. The average over ‘all matrix realizations’ involves nine independent matrix configurations.

## 4. Results and discussion

For the sake of comparison with the previous studies of the MB water model, we adopt the units and values of model parameters as used before [34–39]. The two principal parameters of the MB model are the strength of the ‘hydrogen bond’ interaction,  $\varepsilon_{\text{HB}} = -1$ , and the related bond length  $r_{\text{HB}} = 1$ . The LJ depth of the well  $\varepsilon_{\text{LJ}}$  was the same for all interaction pairs and equal to one-tenth of HB interaction energy  $\varepsilon_{\text{HB}}$  ( $\varepsilon_{\text{LJ}} = 0.1|\varepsilon_{\text{HB}}|$ ), while the Lennard–Jones contact parameter was set to  $\sigma_{\text{LJ}}^{11} = 0.7r_{\text{HB}}$ . All the results are given in reduced units; the excess internal energy and temperature are normal-

ized to the HB interaction parameter  $\varepsilon_{\text{HB}}$  ( $A^* = \frac{A}{|\varepsilon_{\text{HB}}|}$ ,  $T^* = \frac{k_{\text{B}} \times T}{|\varepsilon_{\text{HB}}|}$ ) and all the distances are scaled to

the characteristic length  $r_{\text{HB}}$  ( $r^* = \frac{r}{r_{\text{HB}}}$ ). During this study we varied the size of the matrix particles from  $\sigma_{\text{LJ}}^{00} = 1.0r_{\text{HB}}$  to  $5.0r_{\text{HB}}$ , with the bulk of the computations being performed for  $\sigma_{\text{LJ}}^{00} = 5.0r_{\text{HB}}$ .

### 4.1. Pair distribution functions

Figs. 2–6 give the resulting pair distribution functions for MB water in the Lennard–Jones confinement, given

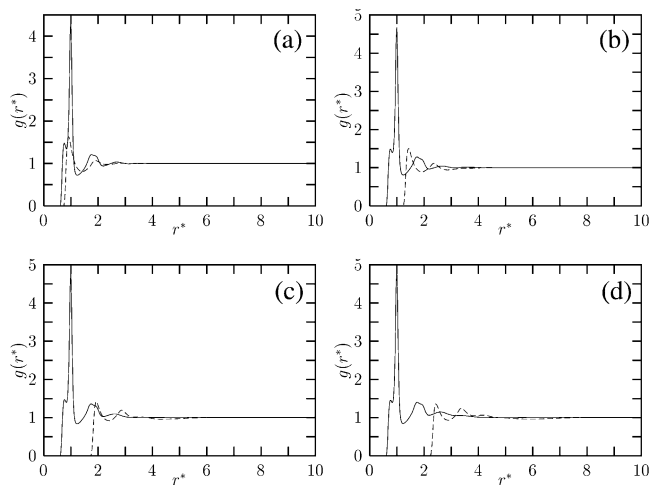


Fig. 3. The fluid–fluid and fluid–matrix distribution functions for  $T_0^* = T_1^* = 0.24$ ,  $\rho_1^* = 0.4$ , and  $\rho_0^* \sigma_{\text{LJ}}^{00} = 0.25$ : (a)  $\sigma_{\text{LJ}}^{00} = 1.0r_{\text{HB}}$ , (b)  $\sigma_{\text{LJ}}^{00} = 2.0r_{\text{HB}}$ , (c)  $\sigma_{\text{LJ}}^{00} = 3.0r_{\text{HB}}$ , and (d)  $\sigma_{\text{LJ}}^{00} = 4.0r_{\text{HB}}$ . The fluid–fluid distribution functions are given by full lines and the fluid–matrix distribution functions are given by broken lines.

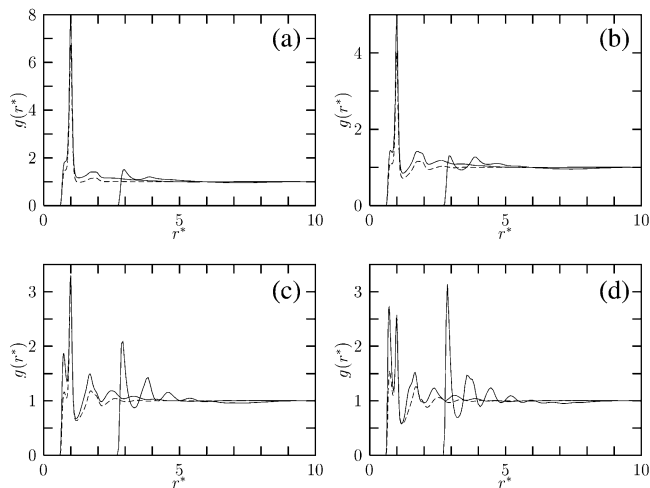


Fig. 4. The fluid–fluid and fluid–matrix distribution functions for  $T_0^*=T_1^*=0.24$ ,  $\sigma_{LJ}^{00}=5.0r_{HB}$  and  $\rho_0^*=0.01$ : (a)  $\rho_1^*=0.1$ , (b)  $\rho_1^*=0.4$ , (c)  $\rho_1^*=0.8$ , and (d)  $\rho_1^*=1.1$ . The pair distribution functions for MB fluid in matrix are given by full lines and the results for unperturbed MB fluid are given by broken lines.

by Eqs. (22) and (23). Fig. 2 shows the fluid–fluid (panels a and b) and fluid–matrix distribution (c and d) functions as obtained by computer simulation and by the associative replica OZ theory described in Section 3. We studied LJ particles with size equal to  $\sigma_{LJ}^{00}=1.0r_{HB}$ . We studied systems for which  $T_0^*=T_1^*=0.24$ ,  $\rho_0^*=0.2$ , and for values of  $\rho_1^*$  equal to 0.4 and 1.0. The comparison between the Monte Carlo (symbols) and associative replica OZ calculations (lines) indicates that the predictions of associative replica OZ theory are reasonably accurate, at least, for these values of concentrations, temperatures, and other model parameters. This is quite encouraging since the Monte Carlo study requires orders of magnitude more computer time than the associative replica calculation of the same model system. Consistent with the results of the previous studies [37–39], the approximate theory, using the orientation-averaged Mayer function for the HB part of the pair potential (Eq. (3)), predicts the fluid–fluid structure to be of shorter range than what is observed in the MC simulations.

Fig. 3 shows the effect of varying the sizes of the LJ obstacles. The associative replica OZ results for fluid–fluid and fluid–matrix distributions are shown for (a)  $\sigma_{LJ}^{00}=1.0r_{HB}$ ; (b)  $\sigma_{LJ}^{00}=2.0r_{HB}$ ; (c)  $\sigma_{LJ}^{00}=3.0r_{HB}$ ; and (d)  $\sigma_{LJ}^{00}=4.0r_{HB}$ . Other parameters are:  $T_0^*=T_1^*=0.24$ ,  $\rho_1^*=0.4$ , and  $\rho_0^*\sigma_{LJ}^{002}=0.25$ . The conclusion is that the HB peak at  $r^*=1$  slightly increases by increasing the magnitude of  $\sigma_{LJ}^{00}$ , keeping all other parameters unchanged.

The results shown in Figs. 4–6 are obtained for larger obstacles, having  $\sigma_{LJ}^{00}=5.0r_{HB}$ . Fig. 4 shows the fluid–fluid and fluid–matrix distribution functions for  $T_0^*=T_1^*=0.24$ , and  $\rho_0^*=0.01$ ; (a)  $\rho_1^*=0.1$ ; (b)  $\rho_1^*=0.4$ ; (c)

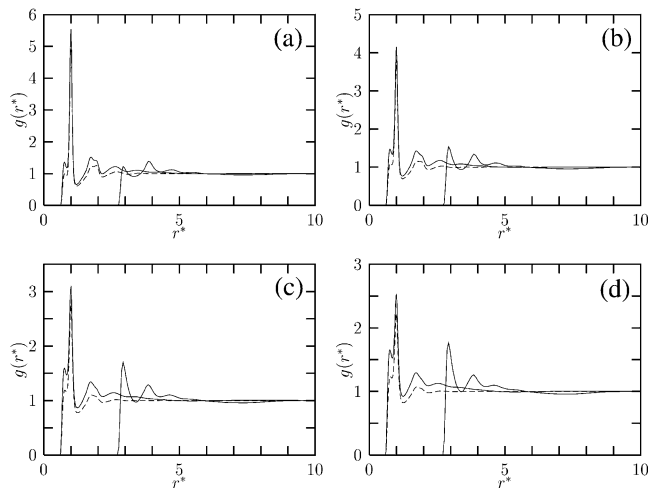


Fig. 5. The fluid–fluid and fluid–matrix distribution functions for  $\rho_1^*=0.55$ ,  $\sigma_{LJ}^{00}=5.0r_{HB}$  and  $\rho_0^*=0.01$ : (a)  $T_1^*=0.20$ , (b) 0.24, (c) 0.30, and (d) 0.36. Notation as for Fig. 4,  $T_0^*=0.24$ .

$\rho_1^*=0.8$ ; and (d)  $\rho_1^*=1.1$ . The pair distribution functions for HB model water in the matrix are given by full lines, and the results for the bulk fluid are shown by broken lines. In general, the pair distribution function of the confined fluid shows more structure than that of the unperturbed one (broken line) for all the densities shown here. The result is consistent with the previous studies of solvation of non-polar solute by MB molecules [34], and also with observations of the recent study of a water-like fluid in a disordered microporous material [42]. The first peak in the fluid–fluid distribution function (the LJ peak) increases by increasing  $\rho_1^*$ , while the HB peak (located at  $r^*=1$ ) decreases during this process. The fluid–matrix distribution has its peak around  $r^*=2.8$ , and the peak strongly increases with the increasing density of MB water. For a high concentration of the adsorbed fluid (see panel d), the LJ peak gets higher than the HB peak, which is a sign of strong

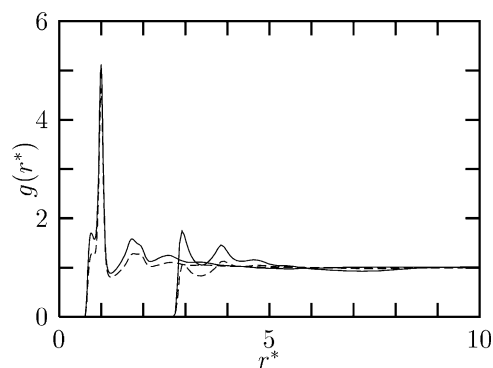


Fig. 6. The fluid–fluid and fluid–matrix distribution functions for  $T_0^*=T_1^*=0.24$ . By broken lines, we show the results for  $\rho_0^*=0.005$ , and by full lines for  $\rho_0^*=0.015$ ,  $\sigma_{LJ}^{00}=5.0r_{HB}$  and  $\rho_1^*=0.4$ .

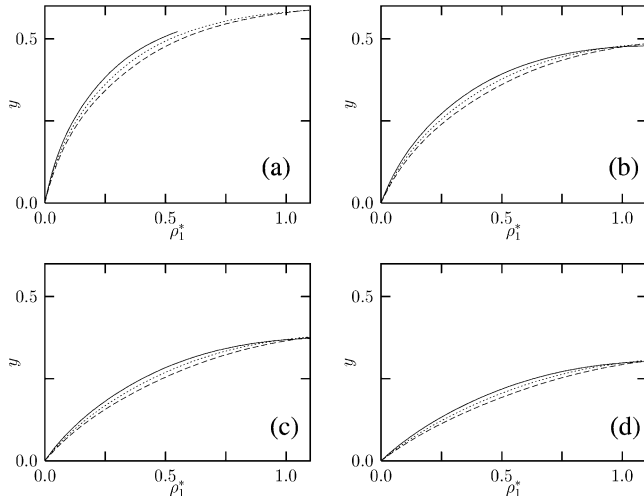


Fig. 7. Fraction of bonded model water molecules  $y = 1 - x$  as a function of the density of the adsorbed MB fluid  $\rho_1^*$  at (a)  $T_1^* = 0.20$ , (b)  $0.24$ , (c)  $0.30$ , and (d)  $0.36$ , respectively. By broken lines, we show the results for bulk MB fluid at this temperature, by dotted lines we show the results for  $\rho_0^* = 0.005$ , and by full lines we show the results for  $\rho_0^* = 0.01$ ;  $\sigma_{LJ}^{00} = 5.0r_{HB}$ , and  $T_0^* = 0.24$ .

adsorption of the water molecules to the surfaces of the obstacles.

Fig. 5 shows the effect of the observation temperature on the various distribution functions. For comparison, the broken lines show the same quantity for the MB model fluid with no obstacles present: panel (a)  $T_1^* = 0.20$ ; (b)  $T_1^* = 0.24$ ; (c)  $T_1^* = 0.30$ ; and (d)  $T_1^* = 0.36$ . These results apply to  $\rho_0^* = 0.01$ ,  $\rho_1^* = 0.55$ ,  $T_0^* = 0.24$ , and  $\sigma_{LJ}^{00} = 5.0r_{HB}$ . Again, the fluid confined in the matrix (full lines) shows more structure than the bulk fluid. The probability for the MB model molecule to form a hydrogen bond (see peak at  $r^* = 1$ ) decreases with the increasing temperature, similarly to that of the bulk fluid. It is interesting, however, to see how the fluid–matrix distribution function changes with temperature  $T_1^*$ . At low temperature of observation (panel a) the second peak of the fluid–matrix distribution function located around  $r^* = 4$  is higher than the first one. The fluid molecules form a cage around the obstacle; they want to make as many hydrogen bonds with neighboring MB molecules as possible. With the increasing temperature, the first peak of the fluid–matrix distribution function (located at  $r^* \approx 2.8$ ) increases; i.e. more MB ‘waters’ adsorb to the obstacles at higher  $T_1^*$  (panel d). Finally, Fig. 6 shows the effect of the matrix density on the interparticle correlation. Here we present the fluid–fluid and fluid–matrix distribution functions at  $\rho_1^* = 0.4$ , and  $T_0^* = T_1^* = 0.24$ , but for two different values of matrix concentration ( $\sigma_{LJ}^{00} = 5.0r_{HB}$ ). The continuous curve is for  $\rho_0^* = 0.015$ , and the broken curve is for matrix density  $\rho_0^* = 0.005$ .

#### 4.2. Fraction of hydrogen bonded MB molecules

Using the associative ROZ, we calculated the fraction of fluid molecules,  $y = 1 - x$ , that form at least one hydrogen bond (see Eq. (19)). All the results presented in this subsection apply to large obstacles,  $\sigma_{LJ}^{00} = 5.0r_{HB}$ . Fig. 7 shows  $y$  as a function of the density of adsorbed fluid  $\rho_1^*$  at matrix densities  $\rho_0^* = 0.005$  (dotted lines) and  $\rho_0^* = 0.01$  (full lines). For comparison, we also show (broken lines) the same quantity for bulk fluid (with no obstacles present): panel (a)  $T_1^* = 0.20$ ; (b)  $T_1^* = 0.24$ ; (c)  $T_1^* = 0.30$ ; and (d)  $T_1^* = 0.36$ . In all four cases,  $T_0^* = 0.24$ . The results indicate that the probability of forming a bond is generally higher in the confined system with  $\rho_0^* = 0.01$  than for the corresponding bulk liquid, except at very high fluid and/or matrix densities. This is in agreement with the results for the pair correlation functions shown in the previous subsection. For the lowest temperature of observation studied here,  $T_1^* = 0.20$ , we have not been able to obtain convergent solutions for all the annealed fluid densities up to 1.1. That is why the curve for  $T_1^* = 0.20$  and  $\rho_0^* = 0.01$ , shown in in panel Fig. 7a (and in Fig. 9a and Fig. 10a), stops at fluid densities around  $\approx 0.55$ .

How does the matrix density affect ‘hydrogen bonding’ of MB molecules? Fig. 8 shows the ratio  $y/y(0)$  as a function  $\rho_0^*$ .  $y(0)$  is the fraction of bonded molecules in the unperturbed (bulk) fluid, and  $y$  is the same quantity in the presence of obstacles. The results are for  $T_1^* = T_0^* = 0.28$ ;  $\sigma_{LJ}^{00} = 5.0r_{HB}$ , and with the MB fluid concentration  $\rho_1^* = 0.6$  (broken line), or 1.0 (full line), respectively. The ratio  $y/y(0)$  strongly depends on the MB fluid density. For low fluid densities (broken line), hydrogen bonding increases with matrix density. For higher MB fluid densities (full line),  $y/y(0)$  increases to a maximum, then decreases upon further increases of  $\rho_0^*$ . It is clear ( $y/y(0) < 1$ ), that for high matrix and fluid densities the fraction of bonded molecules is smaller than in the unperturbed fluid. At high matrix densities,

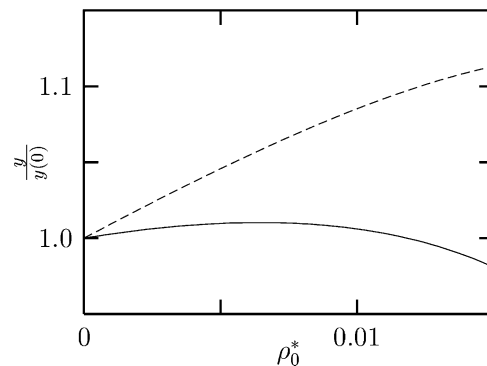


Fig. 8. The ratio of bonded MB waters,  $y/y(0)$ , as a function of matrix density  $\rho_0^*$ . The fluid concentration  $\rho_1^*$  is 0.6 (broken line), and 1.0 (full line); in both cases  $T_1^* = T_0^* = 0.28$ ;  $\sigma_{LJ}^{00} = 5.0r_{HB}$ .

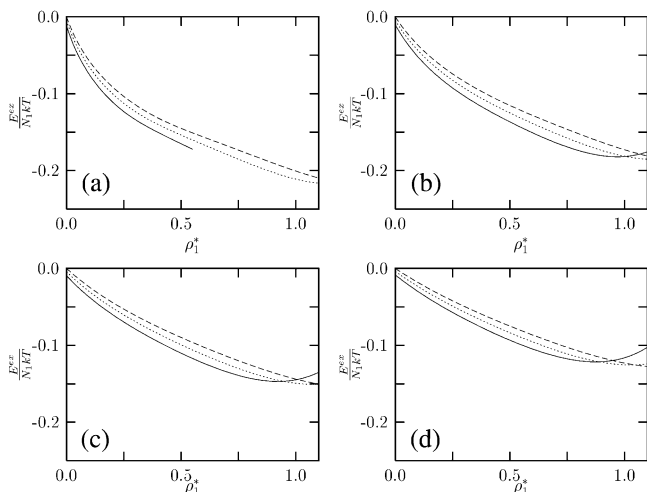


Fig. 9. Reduced excess internal energy as a function of  $\rho_1^*$  at (a)  $T_1^*=0.20$ , (b) 0.24, (c) 0.30, and (d) 0.36, respectively. By broken lines, we show the results for bulk water at this temperature, by dotted line the results for  $\rho_0^*=0.005$ , and by full lines the results for  $\rho_0^*=0.01$ ; in all cases  $T_0^*=0.24$ ,  $\sigma_{LJ}^{00}=5.0r_{HB}$ .

the matrix occupies most of the volume in the system, so MB molecules are unable to form good hydrogen bonding structures.

In the present calculation, it is assumed that the distribution of matrix particles is given by an equilibrium distribution at temperature  $T_0^*$ . Therefore, this temperature influences the interparticle correlations in the matrix. We have explored the effect of varying  $T_0^*$  on the fraction of bonded fluid molecules. For the range of model parameters, temperatures and concentrations studied in this work, the effect of  $T_0^*$  is small and, therefore not shown here. This result is in contrast to the studies of partly quenched ionic systems [56,57], where the observable properties very strongly depend on the temperature of matrix preparation  $T_0^*$ .

#### 4.3. Excess internal energy and the isothermal compressibility

Knowledge of the correlation functions, shown in the previous subsection, allows us to calculate the thermodynamic properties of the system. In this paper, we present the excess internal energy  $E^{ex}$ , and the isothermal compressibility. The reduced excess internal energy per particle is given by the expression:

$$\begin{aligned} \frac{\beta_1 E^{ex}}{N_1} &= 2\pi\rho_0\beta_1 \int g^{10}(r)U_{LJ}^{10}(r)rdr \\ &+ \pi\rho_1\beta_1 \int (g^{11}(r)U_{LJ}^{11}(r) + 9x^2 g_{00}^{11}(r) \\ &< U_{HB}(r, \theta_1, \theta_2) e^{-\beta U_{HB}(r, \theta_1, \theta_2)} >_{\theta_1, \theta_2}) r dr. \end{aligned} \quad (24)$$

The first term in this equation represents the fluid–matrix contribution, and the second represents the fluid–fluid contribution to the excess internal energy of the system [37].

Fig. 9 shows the excess internal energy as a function of the MB fluid density  $\rho_1^*$ . The results for pure fluid (no obstacles present) are shown by broken lines, the results for  $\rho_0^*=0.005$  by dotted, and for  $\rho_0^*=0.01$  by full lines ( $\sigma_{LJ}^{00}=5.0r_{HB}$ ). Panel (a) shows the results for  $T_1^*=0.20$ ; (b) for  $T_1^*=0.24$ , (c) for  $T_1^*=0.30$  and (d) for  $T_1^*=0.36$ . For all these examples,  $T_0^*=0.24$ . The excess internal energy of the confined fluid is more negative than the same quantity for the unperturbed fluid, consistent with more hydrogen bonding in the confined fluid. This is not true for high fluid and matrix densities, especially at higher temperatures. For high matrix density  $\rho_0^*=0.01$ , the excess internal energy first decreases with the increasing density of the adsorbed MB fluid and after reaching the minimum increases again.

We also studied the isothermal compressibility. The reduced isothermal compressibility  $[\partial\rho_1/\partial\times(\beta_1 P)]_{T_1}$  was calculated according to the equation [58]:

$$\left[ \frac{\partial\rho_1}{\partial(\beta_1 P)} \right]_{T_1} = 1 + \rho_1 \int dr h^{11,c}(r), \quad (25)$$

where  $h^{11,c}(r)$  is the connected part of the fluid–fluid correlation function.

Fig. 10 shows the reduced isothermal compressibility as a function of the density of adsorbed MB fluid  $\rho_1^*$ . Panel (a) shows the results for  $T_1^*=0.20$ , (b) for  $T_1^*=0.24$ , (c) for  $T_1^*=0.30$ , and (d) for  $T_1^*=0.36$ . The results for unperturbed MB water are shown by broken lines,

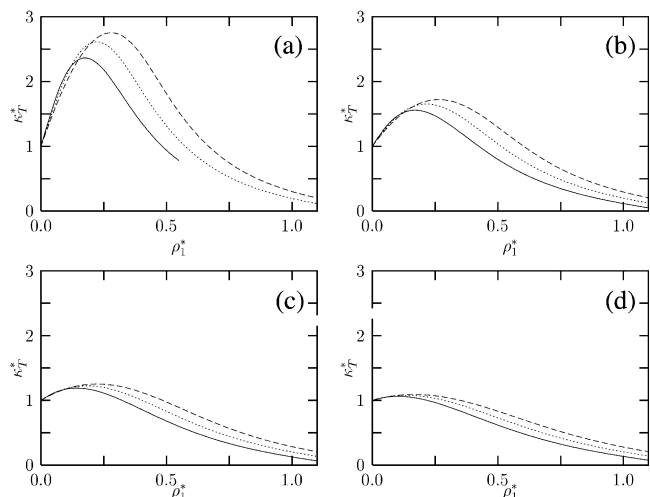


Fig. 10. Isothermal compressibility as a function of  $\rho_1^*$  at (a)  $T_1^*=0.20$ , (b) 0.24, (c) 0.30, and (d) 0.36, respectively. Notation and parameters as for Fig. 9.

and the matrix results are shown with the dotted ( $\rho_0^* = 0.005$ ) and full lines ( $\rho_0^* = 0.01$ ,  $\sigma_{LJ}^0 = 5.0r_{HB}$ ). For all these examples,  $T_0^* = 0.24$ . The isothermal compressibility of the confined fluid is, for low values of  $\rho_1^*$ , slightly larger than the same quantity for unperturbed fluid. The situation is different at high densities  $\rho_1^*$ , where the isothermal compressibility of the confined MB water is considerably lower than that of the unperturbed model water. This picture confirms that the temperature of observation is an important parameter; the compressibility of warm MB water is less affected by the presence of obstacles than for cold water.

## 5. Conclusions

In this work, we studied how fixed obstacles affect the structure and thermodynamic properties of water, using the simple two-dimensional MB model of water, and with quenched Lennard–Jones disks as the obstacles. The matrix of obstacles is prepared from an equilibrium distribution of LJ fluid at temperature  $T_0^*$ , which can be different from the temperature of observation  $T_1^*$ . We explore this model using the associative replica Ornstein–Zernike equation, supplemented by the corresponding hypernetted chain closure approximation. Also, we test some model conclusions using Monte Carlo simulations.

We find that adding a few obstacles to MB water (i.e. low obstacle density) induces local structuring in the fluid, increasing the MB water–water ‘hydrogen bonding’, and increasing the isothermal compressibility, compared to the pure fluid. MB water forms cages around the LJ solutes. This conclusion is consistent with experiments [8] and with the conclusions of Kovalenko and Hirata [42], who studied an extended SPC model water adsorbed into a microporous material prepared from the obstacles of about the same size as the model water. We also find, however, that the further increase of the obstacle density to the point where the obstacles occupy a large fraction of the space in the system, leads to a decreased water ordering, hydrogen bonding, and isothermal compressibility. These conclusions may be important for water inside biological cells, which have a high degree of molecular crowding from organelles and high concentrations of biomolecules.

One of the main shortcomings of this calculation is the use of the orientationally averaged function for the HB part of the fluid–fluid interaction potential. The same approximation has previously been applied to the pure MB fluids [37], and to the mixtures with Lennard–Jones solute [38]. By comparison with the Monte Carlo simulations for bulk model water, we found that the orientationally averaged solution of the associative OZ is a good approximation above  $T_1^* = 0.22$ , and for reduced MB water densities around  $\rho_1^* = 1.0$ . Hence, most of the calculations presented in this work apply to

$T_1^* = 0.24$  or higher. Recently, a more exact orientation-dependent version of the associative OZ has been developed [39], and we hope to extend that approach to the partly quenched systems of the type we study here.

## Acknowledgments

This work was supported by NIH grant GM63592-02, and in part by the Ministry of Science of Slovenia (Theoretical Chemistry 0103-505). O.P. acknowledges support of DGAPA of the National University of Mexico (UNAM) under Grant No. IN113201 and CONACyT of Mexico under Grant No. 37323E.

## References

- [1] S.H. Chen, M.C. Bellissent-Funnel, Hydrogen bond networks, in: M.C. Bellissent-Funnel, J.C. Dore (Eds.), NATO ASI Series C: Mathematical and Physical Science 435, Kluwer Academic Publishers, 1994, p. 337.
- [2] L.R. Pratt, A. Pohorille, Chem. Rev. 102 (2002) 2671–2691.
- [3] M.S.P. Sansom, I.H. Shrivastava, K.M. Ranatunga, G.R. Smith, Trends Biochem. Sci. 25 (2000) 368–374.
- [4] P.M. Wiggins, Cell Mol. Biol. 47 (2001) 735–744.
- [5] M.C. Bellissent-Funnel, R. Sridi-Dorbez, L. Bosio, J. Chem. Phys. 104 (1996) 10 023–10 029.
- [6] F. Bruni, M.A. Ricci, A.K. Soper, J. Chem. Phys. 109 (1998) 1478–1485.
- [7] A.K. Soper, F. Bruni, M.A. Ricci, J. Chem. Phys. 109 (1998) 1486–1494.
- [8] J.C. Dore, Chem. Phys. 258 (2000) 327–347.
- [9] A. Scodinu, J.T. Fourkas, J. Phys. Chem. B 106 (2002) 10 292–10 295.
- [10] V. Crupi, D. Majolino, P. Migliardo, V. Venutti, J. Phys. Chem. B 106 (2002) 10 884–10 894.
- [11] C. Hartnig, W. Witschel, E. Spohr, P. Gallo, M.A. Ricci, M. Rovere, J. Mol. Liq. 85 (2000) 127–137.
- [12] G. Hummer, J.C. Rasaiah, J.P. Noworyta, Nature 414 (2001) 188–190.
- [13] A. Giaya, R.W. Thompson, J. Chem. Phys. 116 (2002) 2565–2571.
- [14] I. Brovchenko, A. Geiger, J. Mol. Liq. 96 (2002) 195–206.
- [15] A. Berezhkovskii, G. Hummer, Phys. Rev. Lett. 89 (2002) 064503.
- [16] A. Waghe, J.C. Rasaiah, G. Hummer, J. Chem. Phys. 117 (2002) 10 789–10 795.
- [17] L. Maibaum, D. Chandler, J. Phys. Chem. B 107 (2003) 1189–1193.
- [18] O. Pizio, S. Sokolowski, J. Phys. Stud. 2 (1998) 296–321.
- [19] M.L. Rosinberg, Liquid state methods for disordered systems, in: C. Caccamo, J.-P. Hansen, G. Stell (Eds.), New Approaches to Problems in Liquid State Theory, Kluwer, Dordrecht, 1999.
- [20] O. Pizio, Adsorption in random porous media, in: M. Borowko (Ed.), Computational Methods in Surface and Colloid Science, Marcel Dekker, New York, 2000.
- [21] W.G. Madden, E.D. Glandt, J. Stat. Phys. 51 (1988) 537–558.
- [22] W.G. Madden, J. Chem. Phys. 96 (1992) 5422–5432.
- [23] J.A. Given, G. Stell, J. Chem. Phys. 97 (1992) 4573–4574.
- [24] J.A. Given, G. Stell, Physica A 209 (1994) 495–510.
- [25] J.A. Given, J. Chem. Phys. 102 (1995) 2934–2945.
- [26] H. Tatlipinar, G. Pastore, M.P. Tosi, Philos. Mag. Lett. 68 (1993) 357–361.

- [27] E. Lomba, J.A. Given, G. Stell, J.J. Weis, D. Levesque, Phys. Rev. E 48 (1993) 233–244.
- [28] M.L. Rosinberg, G. Tarjus, G. Stell, J. Chem. Phys. 100 (1994) 5172–5177.
- [29] M.F. Holovko, Z.V. Polishchuk, Condens. Matter Phys. 2 (1999) 267–272.
- [30] A. Ben-Naim, J. Chem. Phys. 54 (1971) 3682–3695.
- [31] A. Ben-Naim, Mol. Phys. 24 (1972) 705–721.
- [32] G. Andoloro, R.M. Sperandeo-Mineo, Eur. J. Phys. 11 (1990) 275–282.
- [33] A.D.J. Haymet, K.A.T. Silverstein, K.A. Dill, Faraday Discuss. 103 (1996) 117–124.
- [34] K.A.T. Silverstein, A.D.J. Haymet, K.A. Dill, J. Am. Chem. Soc. 120 (1998) 3166–3175.
- [35] N.T. Southall, K.A. Dill, J. Phys. Chem. B 104 (2000) 1326–1331.
- [36] K.A.T. Silverstein, K.A. Dill, A.D.J. Haymet, J. Chem. Phys. 114 (2001) 6303–6314.
- [37] T. Urbic, V. Vlachy, Yu.V. Kalyuzhnyi, N.T. Southall, K.A. Dill, J. Chem. Phys. 112 (2000) 2843–2848.
- [38] T. Urbic, V. Vlachy, Yu.V. Kalyuzhnyi, N.T. Southall, K.A. Dill, J. Chem. Phys. 116 (2002) 723–729.
- [39] T. Urbic, V. Vlachy, Yu.V. Kalyuzhnyi, K.A. Dill, J. Chem. Phys. 118 (2003) 5516–5525.
- [40] O. Pizio, Y. Duda, A. Trokhymchuk, S. Sokolowski, J. Mol. Liq. 76 (1998) 183–194.
- [41] A. Kovalenko, O. Pizio, J. Chem. Phys. 108 (1988) 8651–8661.
- [42] A. Kovalenko, F. Hirata, J. Chem. Phys. 115 (2001) 8620–8633.
- [43] J.P. Hansen, I.R. McDonald, Theory of Simple Liquids, Academic, London, 1986.
- [44] Yu.V. Kalyuzhnyi, P.T. Cummings, J. Chem. Phys. 104 (1996) 3325–3328.
- [45] E. Vakarin, Y. Duda, M.F. Holovko, Mol. Phys. 90 (1997) 611–623.
- [46] A. Trokhymchuk, O. Pizio, M. Holovko, S. Sokolowski, J. Chem. Phys. 106 (1997) 200–209.
- [47] M.S. Wertheim, J. Stat. Phys. 35 (1984) 19–43, 35–47.
- [48] M.S. Wertheim, J. Stat. Phys. 42 (1986) 459–476, 477–492.
- [49] J.D. Talman, J. Comp. Phys. 29 (1978) 35–48.
- [50] D. Wu, K. Hui, D. Chandler, J. Chem. Phys. 96 (1992) 835–841.
- [51] D. Bratko, A.K. Chakraborty, J. Chem. Phys. 104 (1996) 7700–7712.
- [52] K.S. Page, P.A. Monson, Phys. Rev. E 54 (1996) R29–R32.
- [53] L. Sarkisov, P.A. Monson, Phys. Rev. E 61 (2000) 7231–7234.
- [54] B. Hribar, V. Vlachy, O. Pizio, J. Phys. Chem. B 104 (2000) 4479–4488.
- [55] M.P. Allen, D.J. Tildesley, Computer Simulations of Liquids, Oxford University, New York, 1989.
- [56] B. Hribar, O. Pizio, A. Trokhymchuk, V. Vlachy, J. Chem. Phys. 107 (1997) 6335–6341.
- [57] B. Hribar, O. Pizio, A. Trokhymchuk, V. Vlachy, J. Chem. Phys. 109 (1998) 2480–2489.
- [58] G.A. Orozco, O. Pizio, S. Sokolowski, A. Trokhymchuk, Mol. Phys. 91 (1997) 625–634.